

# ZEUS-3D 3-D Gallery #2: Super-Alfvénic Turbulence

## Introduction

Super-Alfvénic turbulence ( $v_{\text{rms}}/a_{\text{rms}} > 1$ ) is a difficult task for even the most sophisticated MHD algorithms. Padoan & Nordlund (1999) successfully simulate super-Alfvénic turbulence with a staggered-mesh scheme similar in many ways to *ZEUS*. Separately, Collins & Norman and Klein (*private communication*, 2008) find mixed results with zone-centred Godunov schemes, moreso with unsplit schemes than operator-split ones. However, Stone (*pr. comm.*, 2009) claims his unsplit *ATHENA* code can do super-Alfvénic turbulence without problem, though Klein has questioned this (*pr. comm.*, 2009). Regardless, the paucity of literature on this subject at the time of this writing is an indicator of its complexity and controversy.

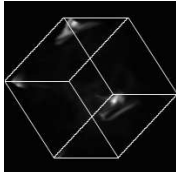
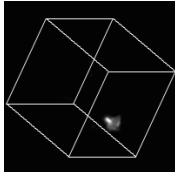
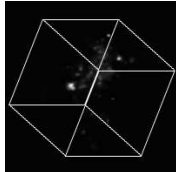
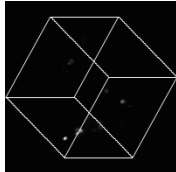
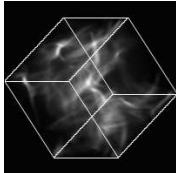
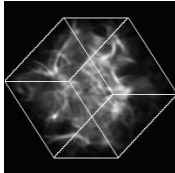
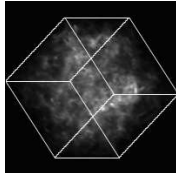
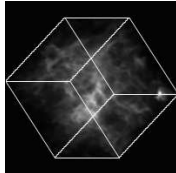
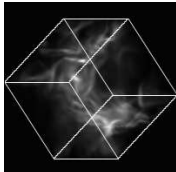
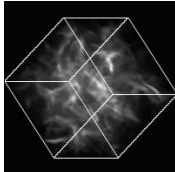
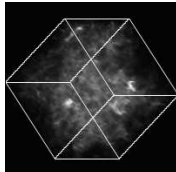
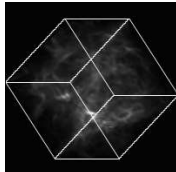
I consider simulations of super-Alfvénic turbulence to be *signatory* of the *Consistent Method of Characteristics* (CMoC; Clarke, 1996, ApJ, 457, 291), an algorithm I developed in the early 90s specifically to combat the explosive instabilities exhibited by Stone & Norman’s original *Method of Characteristics* (MoC; 1992, ApJS, 80, 791) algorithm in my early 3-D jet simulations. Since version 3.2, CMoC has been the primary MHD algorithm in *ZEUS*. On this page, I compare the results of the three MoC-based schemes still supported in *ZEUS-3D*, namely MoC, HSMoC (Hawley & Stone, 1995, JCP, 205, 509), and CMoC, demonstrating the numerical difficulties that can arise. The cause of these difficulties and why CMoC works are discussed in the document [What is planar splitting?](#)

## 64<sup>3</sup> Simulations

The images in Table 0.1 are all line-of-sight integrations of the magnetic pressure ( $p_B = \frac{1}{2}B^2$ ) at the final epochs of 64<sup>3</sup> simulations of isothermal, super-Alfvénic turbulence using three of the four MHD algorithms supported by *Legacy transport* in *ZEUS-3D*. (See the [2-D advection page](#) where the distinction is made between Legacy transport and the new (to Version 3.6) *Finely Interleaved Transport* (FIT) in which only CMoC is supported.) Initially,  $\rho = 1$ ,  $v_{\text{rms}} = 5$ ,  $c_s = 0.1$ ,  $B_x = 10^{-7}$  (in units where  $\mu_0 = 1$ ). Kinetic energy is added to maintain  $v_{\text{rms}} = 1$ .

Turbulence is initialised and driven in specified ranges of the wave-number,  $k$  (box length/wavelength), with the minimum wavelength being two zones. Thus, for a 64<sup>3</sup> simulation,  $1 < k < 32$ . The column headings: low- $k$ ; mid- $k$ ; high- $k$ ; and all- $k$  correspond to:  $1 \leq k \leq 4$ ;  $3 \leq k \leq 4$ ;  $3 \leq k \leq 32$ ; and  $1 \leq k \leq 32$  respectively.

Table 0.1: Animations of  $\int p_B dr$  for 64<sup>3</sup> simulations of super-Alfvénic turbulence driven in four different portions of  $k$ -space using three different MHD algorithms.

	low- $k$	mid- $k$	high- $k$	all- $k$
MoC	 history file spectra	 history file spectra	 history file spectra	 history file spectra
HSMoC	 history file spectra	 history file spectra	 history file spectra	 history file spectra
CMoC	 history file spectra	 history file spectra	 history file spectra	 history file spectra

As shown in Clarke (1996), the MoC is subject to an “explosive-field instability” which is entirely numerical in origin and can drive a  $\beta = 10^{10}$  flow<sup>1</sup> to a  $\beta \sim 1$  flow within a single time step and in a single zone. This can evacuate the zone enough to drive the Alfvén time step to zero, bringing the simulation to a halt. Only the low- $k$  MoC simulation reached  $t = 40$ . The mid- $k$  simulation stopped at  $t = 20$ , and the high- and all- $k$  MoC simulations stopped at  $t \sim 3$ .

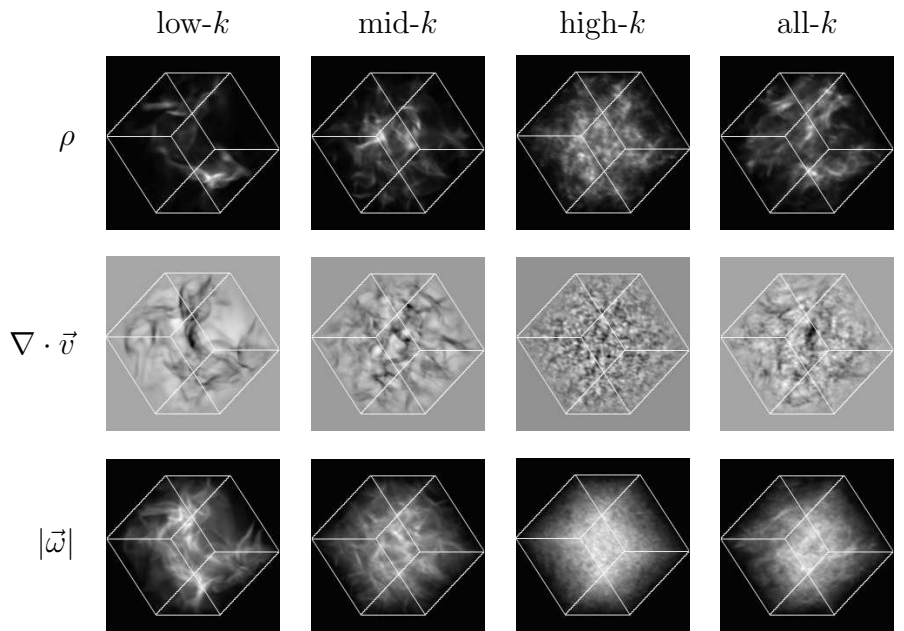
HSMoC and CMoC do not suffer from this instability, and all simulations are run to  $t = 40$  (two sound-crossing times,  $2t_s$ ). The driving  $k$  ranges are apparent in the final images. In the low- $k$  simulations, only the longest wavelengths are driven, causing excessive organisation of the fluid including large voids. Indeed, at  $32^3$  resolution, the fluid becomes organised entirely on a single plane! The mid- $k$  simulations remain filled, and the magnetic field is organised into “filaments”, as has been documented elsewhere. Finally, the high- and all- $k$  simulations show the effects of driving turbulence at the smallest wavelengths, with very fine details appearing in the magnetic field structure. Click on any image in Table 0.1 for an animation.

While there may be little to distinguish the HSMoC and CMoC simulations in Table 0.1, interesting differences in how  $\vec{B}$  grows in time can be found in the history files. When the highest wavenumbers are driven, CMoC exhibits magnetic field “eruptions” during the simulation which can raise the mean magnetic energy density two orders of magnitude higher than the corresponding HSMoC simulation in which the “eruptions” are absent. “Eruptions” are distinct from the MoC “explosions” in that they do not cause excessive decline in the local Alfvén speed, they happen over significant periods of time (tens of time steps), and seem to have a physical basis. In particular, they are associated with localities of strong and sustained shear layers that stretch, and thus strengthen, a weak magnetic field. The shear layer is eventually disrupted but, in some cases, not before the field has grown by an order of magnitude or more. These “eruptions” enrich the rest of the grid with enhanced magnetic field and continue until the overall field strength is sufficient to resist being stretched further.

Why they don’t occur using HSMoC remains a mystery, and may point to numerical problems in CMoC or physical shortcomings in HSMoC. They are absent in both the low- $k$  and mid- $k$  CMoC simulations, and their prominence in high- $k$  CMoC simulations drops as resolution is increased.

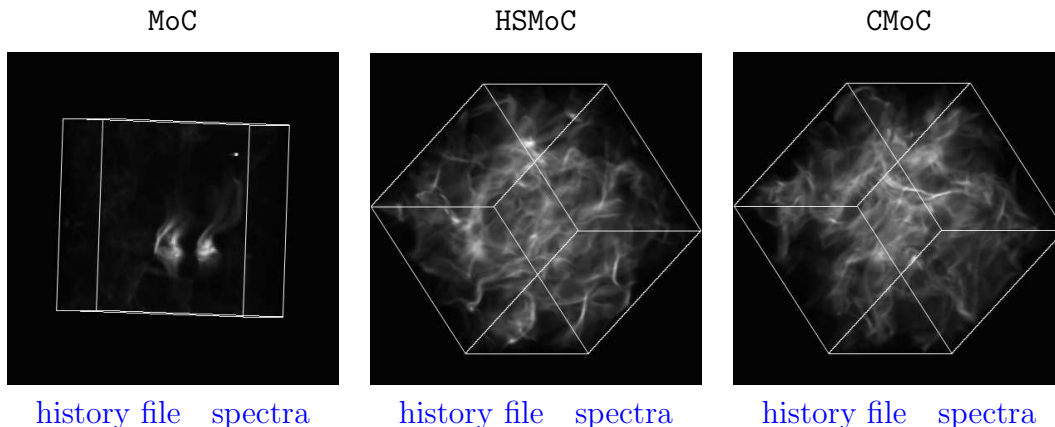
For completeness, links to the animations of line-of-sight integrations of density, velocity divergence, and vorticity magnitude (to indicate shear layers where magnetic filaments are drawn out) for the  $64^3$  simulations are included in Table 0.2 for each of the four driving regimes. Since the HSMoC and CMoC results for these hydrodynamical quantities are very similar, only the CMoC solutions are shown.

Table 0.2: Animations of  $\int \rho dr$ ,  $\int \nabla \cdot \vec{v} dr$ , and  $\int |\vec{\omega}| dr$  for  $64^3$  simulations of super-Alfvénic turbulence driven in four different portions of  $k$ -space using CMoC.



<sup>1</sup> $\beta = p/p_B$ , the *plasma beta*, is the ratio of thermal to magnetic pressure.

Table 0.3: Animations of  $\int p_B dr$  for  $128^3$  simulations of super-Alfvénic turbulence driven in mid- $k$  range for the three different MHD algorithms. Both HSMoC and CMoC runs are shown to  $t = 40$ , whereas the MoC run makes it only to  $t = 14.4$ . Links to the history file and spectra are given below.



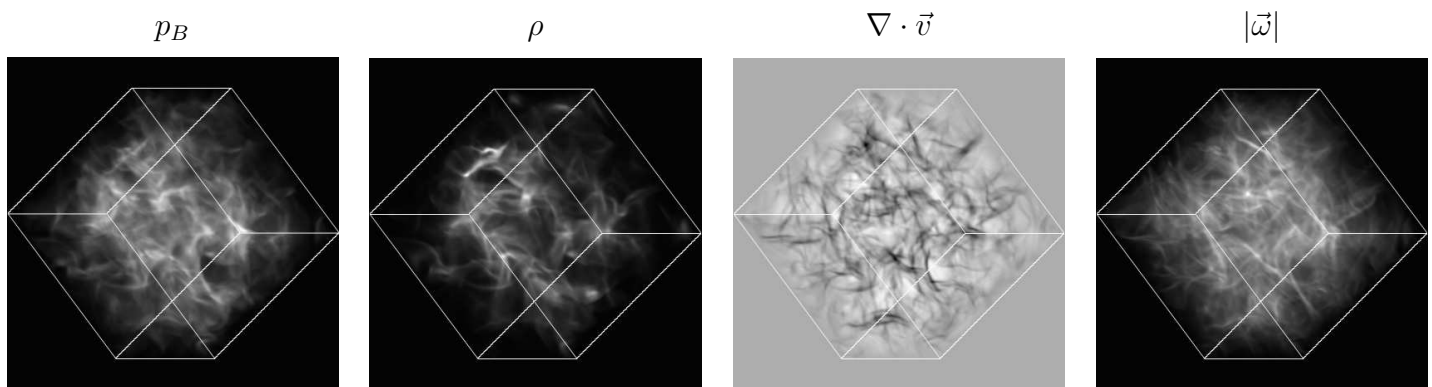
## 128<sup>3</sup> Simulations

Images in Table 0.3 show line-of-sight integrations of the magnetic pressure for the  $128^3$  simulations driven in the mid- $k$  range ( $3 \leq k \leq 4$ ) using the three MHD algorithms. The initial conditions and driving mechanism are the same as the  $64^3$  simulations above. Both the CMoC and HSMoC are shown at  $t = 40$  while the MoC run makes it only to  $t = 14.4$  where it suffers a magnetic explosion (the beginnings of which can be seen as a bright spot in the upper right corner of the cube). While CMoC and HSMoC both give acceptable solutions, HSMoC is not CFL-limited and can become numerically unstable for  $\text{courno} > 0.5$ . By contrast, CMoC can be run with higher values of  $\text{courno}$ ; see the document [What is ZEUS-3D?](#) for further discussion on the MHD algorithms supported in the code.

Table 0.4 displays the same  $128^3$  turbulence simulation taken to  $t = 160$  ( $8t_s$ ) using CMoC for the variables indicated. Click on any image for an animation.

The [history file](#) to  $t = 160$  shows, among other variables, the rms velocities. The rms fluid speed,  $v_{\text{rms}}$ , is initialised at 5 and quickly falls to 1, where it is driven. Since the gas is isothermal, the sound speed,  $c_{\text{rms}}$ , is constant at 0.1 whereas the rms Alfvén speed,  $a_{\text{rms}}$ , increases exponentially from  $t \sim 1$  to  $\sim 120$  until it reaches  $c_{\text{rms}}$  where magnetic growth saturates. The magnetic energy increases by three orders of magnitude between  $0 < t < 1$  during the rapid decline of  $v_{\text{rms}}$ , then by another ten orders of magnitude

Table 0.4: Animations of  $\int p_B dr$ ,  $\int \rho dr$ ,  $\int \nabla \cdot \vec{v} dr$ , and  $\int |\vec{\omega}| dr$  for the same  $128^3$  CMoC simulation in Table 0.3 shown to  $t = 160$ .



between  $1 < t < 120$  ( $6t_s$ ), growing 1.7 orders of magnitude per sound crossing time. At  $t = 120$ , growth halts and the total magnetic energy remains more or less constant through  $t = 160$ . Thus, the system remains supersonic and super-Alfvénic ( $M = M_A = 10$ ), and evolves from  $\beta = 2 \times 10^{13}$  to  $\sim 2$ .

The [Fourier spectra](#) of the variables at the final epoch show a reasonable inertial regime (power law of  $-5/3$ ) in  $3 < k < 25$ , particularly for the density and kinetic energy.

## 256<sup>3</sup> Simulations

Images in [Table 0.5](#) on the next page are of 256<sup>3</sup> super-Alfvénic turbulence simulations at  $t = 40$  with the same initial and driving conditions as the 128<sup>3</sup> simulations using **CMoC**. Similar to the 128<sup>3</sup> simulations, the [history file](#) shows that the magnetic energy density grows at roughly 1.8 orders of magnitude per sound-crossing time, while the [Fourier spectra](#) of the variables at the final epoch show an inertial regime (power law of  $-5/3$ ) in  $3 < k < 40$ , particularly for the density and kinetic energy.

Click on any image for an animation.

## Conclusions

**CMoC**, the *Consistent Method of Characteristics* (Clarke, 1996), has been used in my version of *ZEUS* (and I believe is included in some form in *ZEUSMP* and the *ZEUS* module in *ENZO*) since 1992 without numerical incident<sup>2</sup>. It is a robust 3-D MHD solver whose basis is the concept of *planar*-splitting (better attuned for differencing the curl operator), rather than the traditional *directional*-splitting (better attuned for differencing the divergence operator).

While the algorithm itself is complex and results in rather long and difficult-to-scrutinise subroutines (*e.g.*, see the **CMOC\*** routines in `dzeus36`), this complexity is part and parcel of the planar splitting algorithm which, by its nature, requires *implicit* and *simultaneous* interpolation of four variables on a 2-D plane. Such calculations are time-consuming, but the interpolated values are well-used. Not only are they used to compute the edge-centred emfs, they are used to compute all transverse Lorentz forces, all interpolated momenta required to compute transverse momentum fluxes, and the Poynting flux. Thus, in the end, a simulation using **CMoC** takes no longer to perform than one using the original **MoC** algorithm, since the latter requires separate interpolations for each of these quantities.

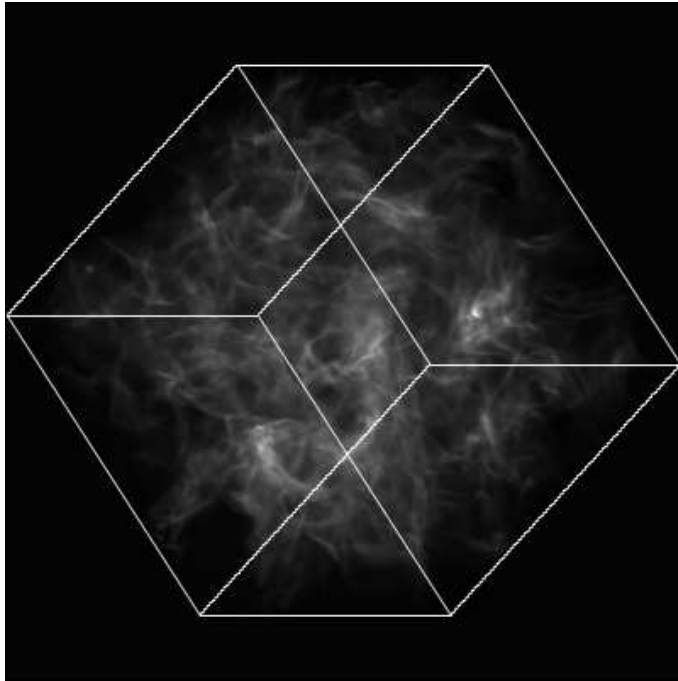
**CMoC** is why *ZEUS-3D* can do any simulation in which super-Alfvénic turbulence plays a role (*e.g.*, any jet simulation with a weak magnetic field, any simulation of the ISM, collapse and fragmentation problems, *etc.*). It is efficient, robust, second order accurate, well-tested, and—best of all—it works!

---

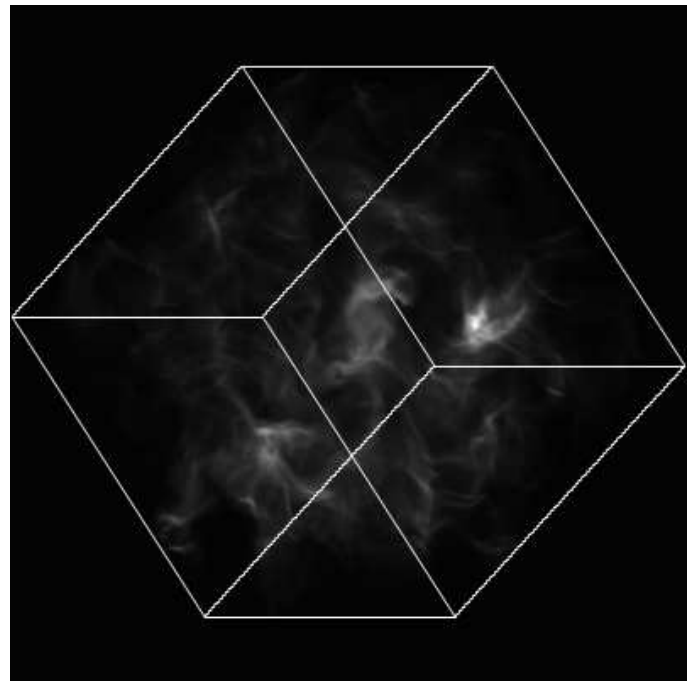
<sup>2</sup>Well, almost. In 2001 I found that I wasn't averaging the densities quite right. This showed up in some shock-tube test problems that were misbehaving at some discontinuities. However, the basis of **CMoC**—planar splitting—remained unaltered. I also had to monkey around with *boundary conditions* in the mid-aughts but again, this had no affect on the actual **CMoC** algorithm which computes the emfs for the *interior* zones.

Table 0.5: Animations of  $\int p_B dr$ ,  $\int \rho dr$ ,  $\int \nabla \cdot \vec{v} dr$ , and  $\int |\vec{\omega}| dr$  for the  $256^3$  CMoC turbulence simulation shown to  $t = 40$ .

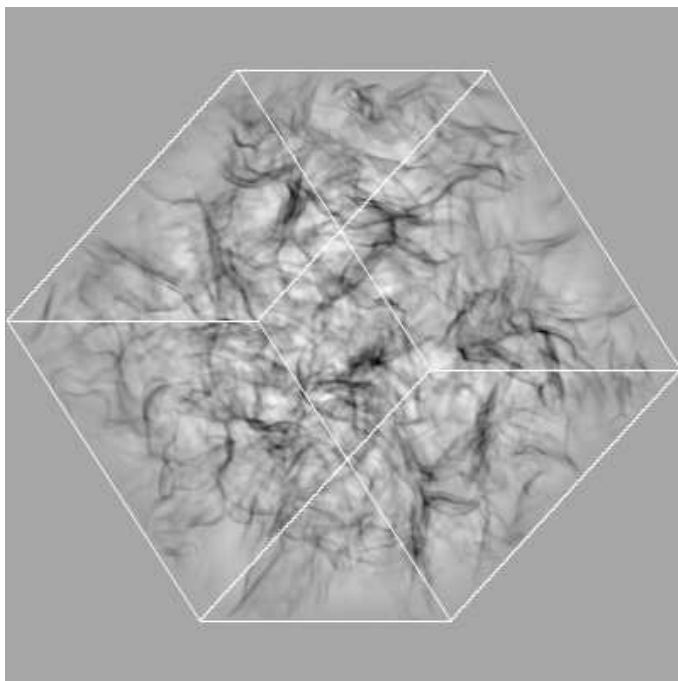
$p_B$



$\rho$



$\nabla \cdot \vec{v}$



$|\vec{\omega}|$

